iScience

Article

# Nano hydroxyapatite-silica with a core-shell structure for long-term management of dentin hypersensitivity

## Graphical abstract

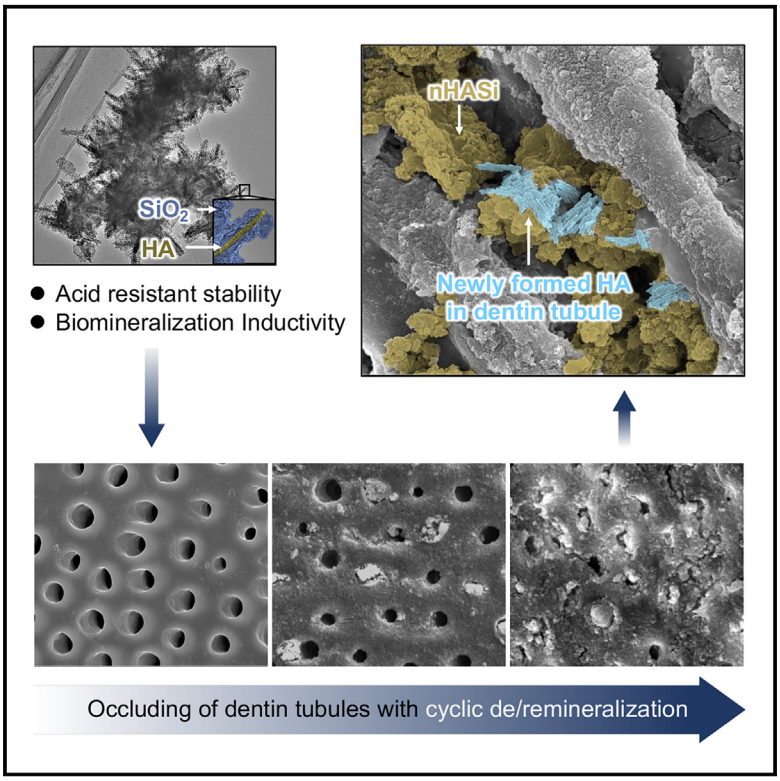


## Highlights

- nHASi releases calcium and phosphate ions from the nHA core for biomineralization
- nHASi exhibits remarkable acid resistance due to the silica shell
- nHASi gradually enhances dentin tubule occlusion over de/remineralization cycles
- nHASi is of excellent cytocompatibility and odontogenic inductivity *in vitro*

## Authors

Yifan Wang, Shangsi Chen, Minjun Zhang, Lili Chen, Chenchen Zhou, Shenglong Tan

## Correspondence

chenlili1030@hust.edu.cn (L.C.), chenchenzhou5510@scu.edu.cn (C.Z.), tansl1989@outlook.com (S.T.)

## In brief

Health sciences; Applied sciences; Materials science

Wang et al., 2024, iScience *27*, 111474
December 20, 2024 
https://doi.org/10.1016/j.isci.2024.111474

CellPress

iScience

CellPress
OPEN ACCESS

Article

# Nano hydroxyapatite-silica with a core-shell structure for long-term management of dentin hypersensitivity

Yifan Wang,[1,2] Shangsi Chen,[3] Minjun Zhang,[4] Lili Chen,[1,2,5,*] Chenchen Zhou,[6,7,*] and Shenglong Tan[8,9,10,*]

[1]School of Stomatology, Tongji Medical College, Huazhong University of Science and Technology, Wuhan 430030, China
[2]Hubei Province Key Laboratory of Oral and Maxillofacial Development and Regeneration, Wuhan 430022, China
[3]Department of Biomedical Engineering, The Chinese University of Hong Kong, Hong Kong SAR 999077, China
[4]College of Life Science and Technology, Huazhong University of Science and Technology, Wuhan 430074, China
[5]Department of Stomatology, Union Hospital, Tongji Medical College, Huazhong University of Science and Technology, Wuhan 430022, China
[6]State Key Laboratory of Oral Diseases, National Clinical Research Center for Oral Diseases, West China Hospital of Stomatology, Sichuan University, Chengdu 610041, China
[7]Department of Pediatric Dentistry, West China Hospital of Stomatology, Sichuan University, Chengdu 610041, China
[8]Stomatology Hospital, Southern Medical University, Guangzhou 510280, China
[9]School of Stomatology, Southern Medical University, Guangzhou 510280, China
[10]Lead contact
*Correspondence: chenlili1030@hust.edu.cn (L.C.), chenchenzhou5510@scu.edu.cn (C.Z.), tansl1989@outlook.com (S.T.)
https://doi.org/10.1016/j.isci.2024.111474

## SUMMARY

Teeth undergo continuous demineralization and remineralization influenced by dietary acid and saliva. Excessive dietary acid attack disrupts this balance, exposing dentin tubules and causing dental hypersensitivity (DH). Due to low acid resistance, traditional anti-DH regents such as calcium phosphate minerals fail in long-term occlusion of dentin tubules, resulting in recurrent attacks of DH. Hence, we fabricate nano hydroxyapatite (nHA)-silica (nHASi) with a core-shell structure that can not only fill in the dentin tubules, releasing $Ca^{2+}$ and $PO_4^{3-}$ from the nHA core for biomineralization, but also exhibit remarkable acid resistance due to the silica shell. Our study demonstrates a continuous growth of hydroxyapatite (HA) nanocrystals within nHASi during cyclic de/remineralization. When applied with toothpaste, nHASi gradually enhances dentin tubule occlusion over de/remineralization cycles. Additionally, extracts of nHASi exhibit excellent cytocompatibility and odontogenic inductivity *in vitro*. This work provides a paradigm for developing effective anti-allergic materials for the long-term management of DH.

## INTRODUCTION

Dentin hypersensitivity (DH) is a common dental disease, especially prevalent in Asia and Europe, affecting 30%–40% of the population.[1,2] DH is manifested as a sharp pain under external stimulations (such as cold, hot, acid, etc.), which alter the fluid flow in the dentin tubules to irritate the pulp nerves,[3] and recovered after removal of the stimulation. Given that the root cause of DH is the exposure of dentin tubules, usually as a result of enamel erosion by dietary acid, sealing exposed dentin tubules is considered to be an effective treatment for DH.[4] Considering the calcium phosphate-based composition of dentin, materials that can provide either calcium and phosphate ions or mineralization sites to induce Ca-P deposition, such as hydroxyapatite (HA),[5] bioactive glass (BG),[6] monetite,[7,8] and mesoporous silica loading $Ca^{2+}/PO_4$,[3–9] have been proved capable of sealing exposed dentin tubules. However, the oral environment is always changing. With the occasional exposure to dietary acid and acid produced by local oral bacteria, the demineralization process by acidic substances and the remineralization process in the normal salivary environment keep circulating on dentin.[10] These sealing materials are easy to be removed by acid etching and re-expose the dentin tubules.[11] Therefore, in addition to filling and sealing the dentin tubule, a long-term effective anti-allergic agent for DH treatment should also fulfill the need for acid resistance.

Carbonated HA is the most essential inorganic component in teeth, with a weight percent of about 70% in dentin and as high as 96% in enamel.[12] The HA in teeth is tightly and regularly arranged with high crystallinity,[13] endowing it with certain wear resistance and acid resistance. In addition, HA is capable of inducing remineralization in the saliva supersaturated in calcium and phosphate ions. Therefore, HA has been used as an anti-sensitizer to seal dentin tubules in many studies. As is known, the dentinal tubule penetrates the entire dentin and is arranged radially from the surface of the pulp to the enamel-dentin boundary, with a diameter of about 2–4 μm.[14] Due to such a small diameter of the dentinal tubule,

currently, synthesized HA with nanosize is considered effective in dentin tubule occlusion. Unlike the highly oriented and crystallized HA in teeth, these synthesized HA nanoparticles are often with low crystallinity and are stacked randomly in the dentin tubules. Besides, the nanosize provides a much greater specific surface area. Together, these characteristics make the solubility of synthesized HA nanoparticles much higher than that of HA in teeth, which results in poor acid resistance. Even if they can accomplish the dentin tubule occlusion, they are easy to be corroded and re-expose the dentin tubules during the acid-mediated demineralization, consequently failing the long-term DH treatment. In addition to HA, BG is another mainstream active ingredient in the commercial anti-allergic toothpaste. Nano-sized BG can infiltrate into and block the dentin tubules and activate ion reaction to form calcium phosphate layer, which finally converts to HA.[15,16] However, this process is very time-consuming, often taking more than 1 week to achieve the desired results.[17] Therefore, confronted with the daily etching by dietary acid, BG can neither afford effective long-term management of DH.

In past few decades, silica particles have been widely used in drug delivery and biomedical engineering.[18–21] The application of silica particles in dentin tubule occlusion has also been reported.[22–25] Similar to BG, the silica particles filled in dentin tubules can provide active sites for calcium and phosphate ions deposition and mineralization, thereby generating a HA layer.[24] More importantly, silica particles are of good acid stability. This explains that in some recent studies, whether using the calcium chloride and phosphoric acid loaded in the mesoporous silica [9] or nano HA (nHA) coated outside the silica microsphere,[26] as the calcium and phosphate ion sources during the cyclic demineralization and remineralization, demonstrated effective occlusion of dentin tubules. Mutually, these studies also confirmed that locally released calcium and phosphate ions could promote the mineral deposition of silica and enhance the acid resistance stability. Inspired by these findings, we hypothesized that encapsulating nHA within silica holds great potential for not only safeguarding the acid resistance of HA filled in dentin tubules but also facilitating the remineralization of outer silica through the release of calcium and phosphate ions from inner HA, thereby achieving optimal occlusion of dentin tubules for long-term management of DH.

As far as we know, to date, no research has been reported on the long-term dentinal tubule occlusion of silica-coated HA under cycling de/remineralization conditions. To this end, we fabricated an nHA-silica (nHASi) composite of core-shell structure, with the inner layer of nHA and the outer layer of nano silica. In this study, we investigated the acid resistance of nHASi and its mineralization capacity under the cyclic demineralization-remineralization condition and tried to elucidate the underlying mechanism. By adding the nHASi hydrosol into the commercial fluoride toothpaste and comparing it with BG-containing toothpaste, we further evaluated the dentin tubule occlusion under the cycling de/-remineralization to verify the promise of the nHASi in long-term DH treatments. Additionally, we demonstrated the biocompatibility and odontogenic inductivity through *in vitro* co-culturing of human dental pulp stem cells (DPSCs) with the extracts from nHASi.

## RESULTS AND DISCUSSION

### Characterization of nHA and nHASi

The X-ray diffraction (XRD) pattern showed that the main phase of both nHA and nHASi was HA, which suggested the silica coating did not alter the phase composition of nHA (Figure 1A). Additionally, non-crystalline scattering was found in nHASi at the range of 20°–25°, indicating the presence of amorphous silica.[26] X-ray fluorescence (XRF) analysis (Figure 1B; Table S1) indicated that the silicon content in nHASi was about 36.39 At %. By calculation, the mass fraction of the silica coating and the HA core in nHASi was approximately 35% and 65%, respectively. It was noticed that the Ca and P atomic ratio of nHA was about 1.84 At % while that of nHASi was about 1.67 At %, close to the typical Ca to P atomic ratio of HA. Given the limitation of XRF, carbon could not be detected. We therefore speculated that the excessive Ca to P ratio of nHA might be attributed to the carbonate substitution of phosphate groups introduced by the carbon dioxide in the air during the synthesis.[27] Regarding nHASi, the silica coating could block the carbon dioxide resulting in HA without carbonate substitution. Further analysis by Fourier transform infrared spectroscopy (FTIR) confirmed the presence of carbonate groups in nHA, as suggested by the bands at 1,410, 1,453, and 1,565 $cm^{-1}$.[28] The exclusive existence of silica in nHASi was also demonstrated by the absorption peak at 800 $cm^{-1}$, which could be assigned to the Si-O-Si vibration absorption[29] (Figure 1C). Scanning electron microscopy (SEM) and transmission electron microscopy (TEM) observation demonstrated that the morphology of nHA was a cluster of rod-like nanoparticles, with a single particle about 100–200 nm in length and 10–20 nm in width (Figures 1D and 1E). Compared with nHA, although the primary morphological characteristics did not alter significantly, there was an obvious coarse coating of amorphous silica encapsulating each HA nanorod of the nHASi (Figures 1F and 1G). The nHA and nHASi of such nanosize were both easy to infiltrate into the dentin tubules (Figure S2). However, nHA tended to be stacked within the dentin tubules, whereas nHASi was found to be tightly attached to the inner wall of the tubules. The coarse coating of amorphous silica may have aggregation effect,[30] which endowed nHASi with higher adhesion to the dentin surface, potentially improving the washout resistance performance to stabilize the tubule filling.

### Ion release and biomineralization of nHA and nHASi

Calcium and phosphate ions releasing from the mineral desensitizer particles are able to penetrate the depths of the dentin tubules and mineralize to form the HA, thus effectively occluding the dentin tubules.[24] In view of this, we investigated the release kinetics of calcium, phosphate, and silicate ions from nHA and nHASi and the biomineralization of nHA and nHASi in artificial saliva (Figure 2). There was a typical two-stage release of both calcium and phosphate ions (Figures 2A and 2B). The first stage (0–12 h) was short and acute, which belonged to a phase of burst release, whereas the second stage (12–168 h) was long and steady, which might be led by a balance between the ion release and the material-induced mineralization that could consume the calcium and phosphate ions in artificial saliva. Further investigation on biomineralization process supported this speculation

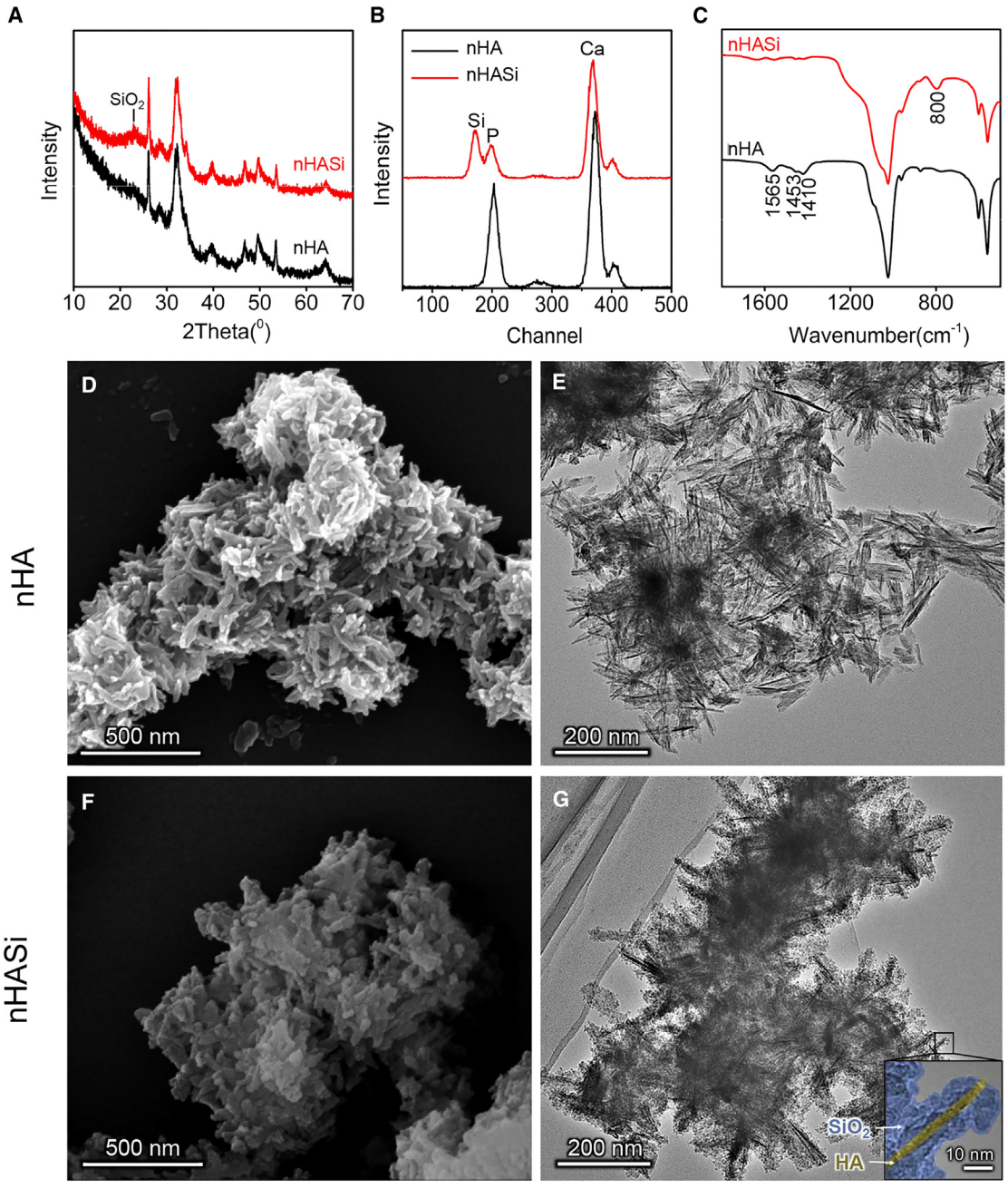


**Figure 1. Characterization of nHA and nHASi**

(A and B) XRD patterns and X-ray fluorescence analysis indicated that hydroxyapatite containing amorphous silica was successfully synthesized.

(C) FTIR results displayed that Si-O-Si vibration absorption peaks at 800 $cm^{-1}$ in nHASi and the obvious $CO_3^{2-}$ groups in nHA.

(D) SEM and (E) TEM image showed that nHA particles were rod-like with length of 100–200 nm and width of 10–20 nm. Scale bar is 500 and 200 nm for SEM and TEM image, respectively.

(F) SEM image showed that the surface of nHASi was rough due to the addition of silica. Scale bar is 500 nm.

(G) TEM (scale bar is 200 nm) and the high-resolution images inserted in the lower right (scale bar is 10 nm) showed that the rod-like HA core of nHASi was encapsulated by the shell of granular amorphous silica.

(Figures 2D–2G). Obvious biomineralization was observed on the surface of nHASi by SEM. After 7 days, numerous short filiform crystals grew out of the coarse silica coating (Figure 2F) and gradually transformed to rod-like nanoparticles after 14 days (Figures 2G and S3). Further XRD analysis (Figure 2H) demonstrated that the phase of the mineralized nHASi was HA. We noticed that the signal intensity of HA decreased over time in nHASi. This may be due to the gradual accumulation of

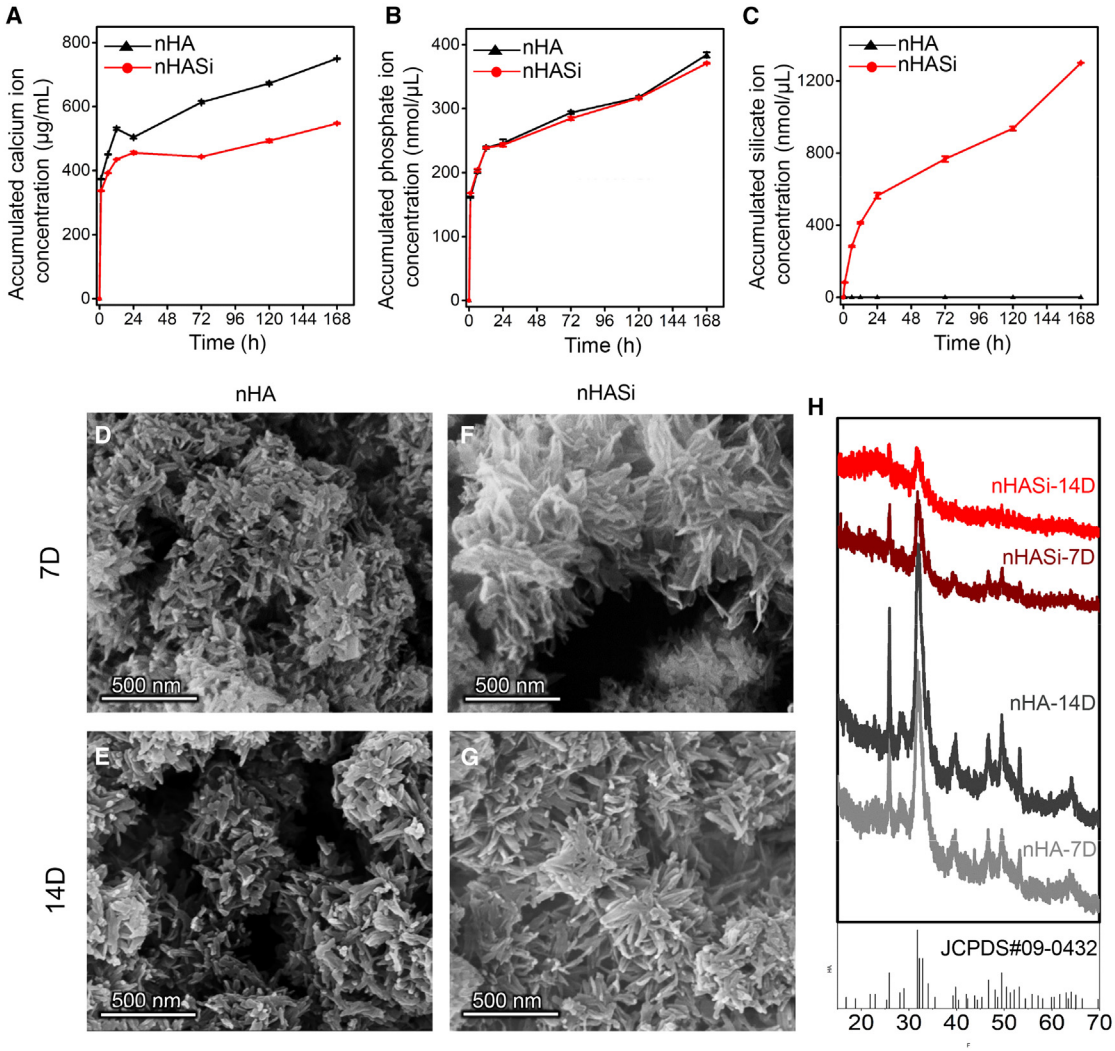


**Figure 2. Accumulated ion releasing and biomineralization of nHA and nHASi in artificial saliva**

(A–H) Accumulated concentration of (A) calcium ions, (B) phosphate ions, and (C) silicate ions in artificial saliva. Data are means ± SD, $n = 3$ parallel samples per group. TEM images of nHA after (D) 7 days and (E) 14 days of mineralization showed rod-like morphology that was almost the same as the nHA before mineralization. Whereas, after 7 days of mineralization, (F) filiform crystals were observed on the surface of nHASi and transformed to (G) rod-like nanoparticles after 14 days. Scale bars are 500 nm. (H) XRD pattern showed that the phases of both mineralized nHA and nHASi were HA.

low crystallinity HA formed during biomimetic mineralization. Regarding nHA, although there was no obvious difference in surface morphology before and after the mineralization, the intensity of HA characteristic peak in XRD patterns increased with the mineralization time, which suggested that nHA may undergo mineralization directly on the basis of its original crystal structure. Additionally, we found the release kinetics of phosphate ions from nHASi was identical with nHA particles, while the accumulation of calcium ions was much slower in the nHASi group (Figures 2A and 2B). This might be caused by the difference in the Ca to P ratio between nHA and nHASi, with the former being significantly higher than the latter (Table S1). More importantly, after soaking in artificial saliva for 7 days, the Ca to P ratio of nHA decreased from about 1.84 to 1.80, whereas that of nHASi increased from 1.67 to 1.70 (Table S1). These changes in Ca to P ratio not only corroborated that nHA released more calcium ions than nHASi but also suggested a dynamic release and remineralization of calcium and phosphate ions in both nHA and nHASi. We also noticed a continuous release of silicate ions from nHASi during the soaking and the corresponding decrease of silicon content in nHASi after 7 days of mineralization (Figure 2C; Table S1). Together, these results indicated that the silica coating of nHASi was soluble in neutral artificial saliva and permeable for calcium and phosphate ions releasing and capable of inducing biomineralization that was beneficial for dentin tubule occlusion.

## Acid resistance of nHA and nHASi

The current desensitizers based on mineral particles such as calcium phosphate, BG, and monetite are usually capable of filling

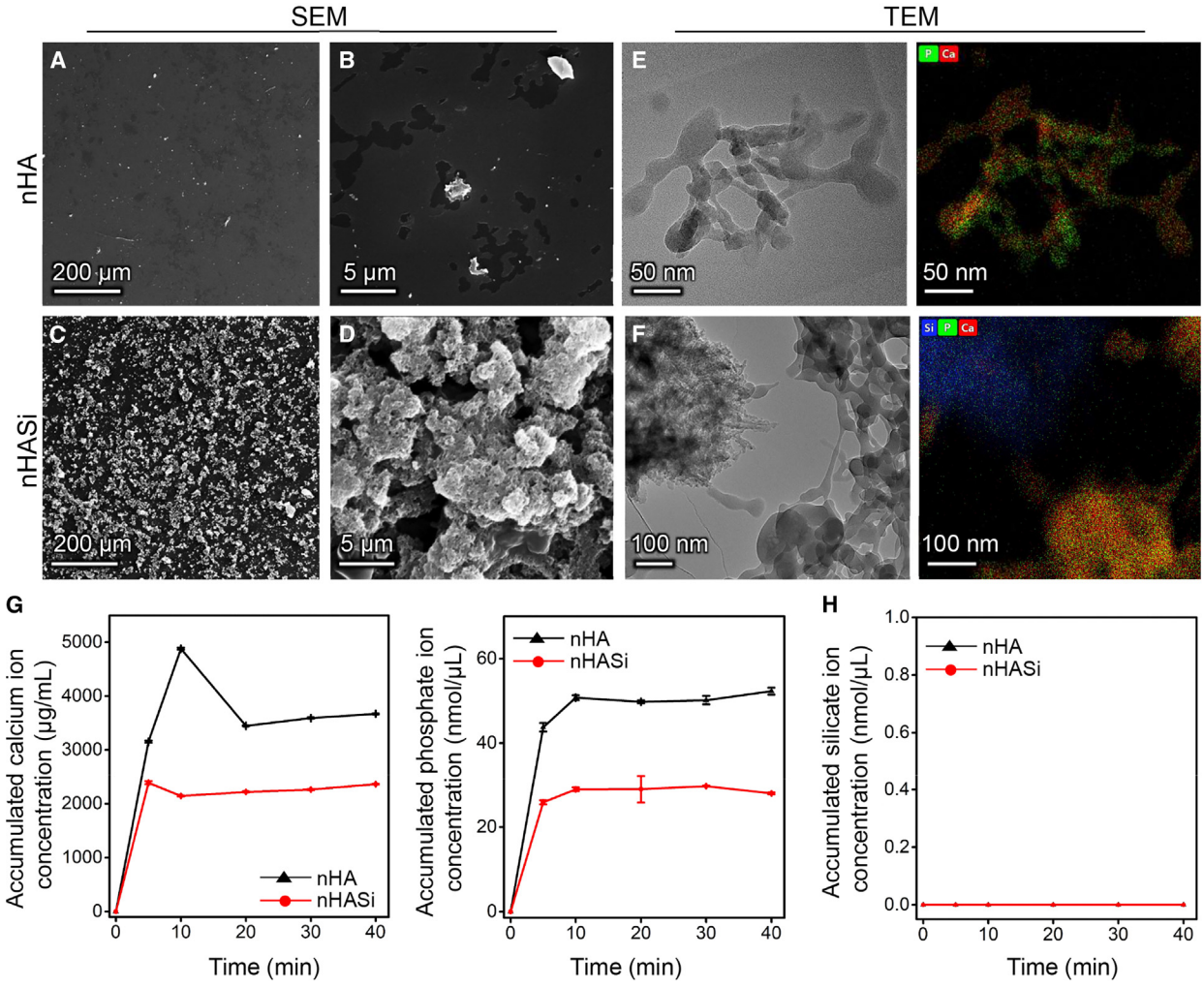


**Figure 3. Acid stability and accumulated ion releasing of nHA and nHASi in 1 wt % citric acid solution**

(A–F) The morphological observation on the remaining particles of (A and B) nHA and (C and D) nHASi after acid treatment by SEM. Scale bars are 200 μm for (A) and (C) and 5 μm for (B) and (D), respectively. (E and F) TEM results indicated that the remaining minerals in nHA and nHASi after acid treatment was amorphous calcium phosphate. Scale bars are 50 nm for (E) and 100 nm for (F), respectively. Notably, the silica coating of nHASi retained the amorphous calcium phosphate within and surrounding itself, which was beneficial for further mineralization.

(G) The accumulated concentration of calcium and phosphate ions in nHASi was lower than that in nHA, suggesting the acid resistance of silica coating.

(H) No silicate ion release was observed from nHASi in citric acid solution. Data are means ± SD, $n$ = 3 parallel samples per group.

and inducing biomineralization within dentin tubules. However, they are likely to be dissolved and dislocated from dentin tubules by the erosion of dietary acid including acidic drinks like cola (pH = 2.6) and vinegar (pH = 3.2),[31] thus failing to realize long-term DH treatment. In view of the acid stability of silica, we coated it on the surface of HA nanoparticles to obtain considerable acid resistance. It has been reported that 1.0 wt % citric acid (pH = 2.23) could ensure the demineralization of mineral particles.[32] Herein, we utilized the 1.0 wt % citric acid to evaluate the acid resistance. As expected, compared with the materials before acid attack (Figures S4 and 1D and 1F), almost all of the nHA particles were dissolved after acid treatment, whereas there were obviously numerous remaining nHASi particles (Figures 3A–3D). Further TEM observation with selected area electron diffraction (SEAD) and elemental mapping showed that, although in both nHA and nHASi, the crystalline HA had almost transformed to amorphous calcium phosphate, the silica coating reserved a considerable amount of calcium phosphate within and surrounding the nHASi particles (Figures 3E, 3F, and S5). Also, the ion release patterns of nHA and nHASi in 1.0 wt. % citric acid (Figures 3G and 3H) demonstrated that the silica coating was insoluble in acid and strongly retarded the release of calcium and phosphate ions from nHASi in comparison with that of nHA. It seemed that the silica coating could not completely protect the inner HA core of nHASi from acid dissolution. This could ascribe to the fact that the HA core in nHASi was quite small, also with low crystallinity, and the citric acid applied herein might be stronger than dietary acid. Nevertheless, the silica coating reserved itself and a great amount of amorphous calcium phosphate after nHASi was eroded (Figure 3F). The bioactivity of

silica rendered it a nucleation site. At the same time, the presence of amorphous calcium phosphate served as a precursor for mineralization, which could synergistically induce biomineralization to facilitate the generation of new HA crystals for long-term effective occlusion of dentin tubules.

### Cycling de/remineralization of nHA and nHASi *in vitro*

In daily life, the mineral particle-based desensitizer for DH would encounter a complex oral environment where demineralization by dietary acid attacks randomly takes place, alongside the mineralization in saliva. Thus, whether biomineralization can be dominant in oral environment determines the effectiveness of the desensitizer mineral particles. Recently, a study reported a composite of BG nanoparticles coated by fluoride-doped amorphous calcium phosphate, which release Ca, P, Si, and F ions to induce mineralization, and thus occlude dentin tubules.[33] However, to the best our knowledge, like this study, the acid resistance of current anti-DH materials, especially in the repeated demineralization and remineralization cycles, has not been fully tested. Herein, a well-designed *in vitro* de/remineralization process[34] was conducted to simulate the complicate environment of the human oral cavity. After 5 days of cyclic treatment with 1 wt % citric acid and artificial saliva, the remaining particles of nHASi were much more than those of nHA, as the coverage area of particles on silicon wafers in the nHASi group was obviously larger than that of the nHA group (Figures 4A–4D). Enlarged SEM images showed that the size of de/remineralized nHASi particles was about 2 μm in width and 3 μm in length, which was much bigger than the nanosized remaining particles of nHA. More importantly, further TEM observation (Figures 4E and 4F) and SEAD (Figure S6) demonstrated that the de/remineralized nHA was purely amorphous, whereas numerous dark dots, which could be newly nucleated calcium phosphate, and a black rod-like crystal that is highly likely to be mineralized HA, were found within the de/remineralized nHASi. We also noticed that the de/remineralization outcomes for both nHA and nHASi depended on the concentration (pH) of the citric acid. When the citric acid concentration was lower than 0.7 wt % (pH $\geq$ 2.30), both nHA and nHASi were able to generate compact rod-like crystals of mineralized HA (Figure S7). However, when the concentration of citric acid reached 0.85 wt % (pH = 2.26), acid-induced demineralization was clearly dominant in nHA, resulting in loss and deformation of the particles (Figures 4G and 4H), while in contrast, remineralization was predominant in nHASi, where dense rod-like HA nanoparticles were observed by SEM and TEM (Figures 4I, 4J, and S8). These results confirmed the aforementioned assumption that the silica coating of nHASi could retain amorphous calcium phosphate during acid erosion and mediate the biomineralization of calcium and phosphate ions in artificial saliva. Considering that the pH value of dietary acid usually exceeds 2.5,[35] our study undoubtedly demonstrated that the nHASi could be effectively remineralized against more extreme acidic conditions.

### Dentin tubule occlusion by nHA and nHASi

To explore whether nHASi could exert an enduring effect on occluding dentin tubules, the nanoparticles were mixed with fluoride toothpaste and compared with pure fluoride toothpaste (F) and commercialized Sensodyne toothpaste (SEN). As shown in Figures 5A–5C, most of the dentin tubules stayed open after 3 days and 5 days of cyclic de/remineralization in F and SEN groups, whereas both of nHA and nHASi exhibited increased occlusion rate with the time of cyclic treatment. Due to the small size and the affinity of hydroxyl groups on nHA/nHASi to dentin, both of nHA and nHASi could easily permeate into the dentin tubules and attach to the dentinal surface, leading to better occlusion rates in F + nHA and F + nHASi groups than that in F and SEN groups. Importantly, the dentin tubule occlusion rate of nHASi was significantly higher than that of nHA after both 3 days and 5 days of cyclic de/remineralization, demonstrating the best acid resistance and the most rapid biomineralization among all groups. Further SEM observation on the longitudinal surface of tubules (Figures 5D–5G) revealed that nHASi not only sealed the openings but also filled up the depth of the dentin tubules, whereas in other groups, only a small amount of mineralized deposits was found in the depth of dentin tubules. Noticeably, rod-like nanocrystals were observed among the mineral deposits within the tubules treated with F + nHASi toothpaste (Figures 5G and S9), suggesting effective mineralization of nHASi to form HA, even under the repetitive citric acid attack. On the other hand, due to the poor acid tolerance, nHA and BG in SEN group could not perform a satisfactory manner in long-term dentin tubule occlusion, which is consistent with previous studies.[36,37] Together, these results indicated that nHASi could constantly induce and consecutively accumulate biomineralization in the complex oral environment that is occasionally attacked by dietary acid, showing great promise in long-term DH treatment.

### Cytocompatibility and odontogenic inductivity evaluations of nHA and nHASi

Biocompatibility and bioactivity are the key factors to be considered for the translational application of DH treatment materials. Given that nHA and nHASi, after occluding the dentin tubules, tend to dissolve and release calcium, phosphate, and silicate ions in the oral environment, thereby affecting the cells within dentin and pulp cavities such as DPSCs and odontoblasts, we used the material extracts for the following research. DSPCs are easy to obtain and have a high potential to undergo odontogenic differentiation to become odontoblasts,[7] thereby facilitating the generation of new dentin and enhancing the restoration of impaired dentin tubules. Therefore, DSPCs were selected for the *in vitro* cytocompatibility and odontogenic inductivity evaluation. The CCK-8 results (Figures 6A and 6B) showed that, despite the slightly lower optical density (OD) values of nHA and nHASi groups compared to the blank group when the concentration of material extracts exceeded 6,250 μg/mL, all groups exhibited an increase in OD values over time, indicating sustained proliferation of DSPCs under all experimental conditions. Noticeably, when the concentration of extract was less than 3,125 μg/mL, nHASi even slightly promoted the proliferation of DSPCs. These findings suggest that both nHA and nHASi are of favorable cytocompatibility. We noticed that when the concentration of extract was 3,125 μg/mL, the cell viability of the nHA and nHASi groups was basically

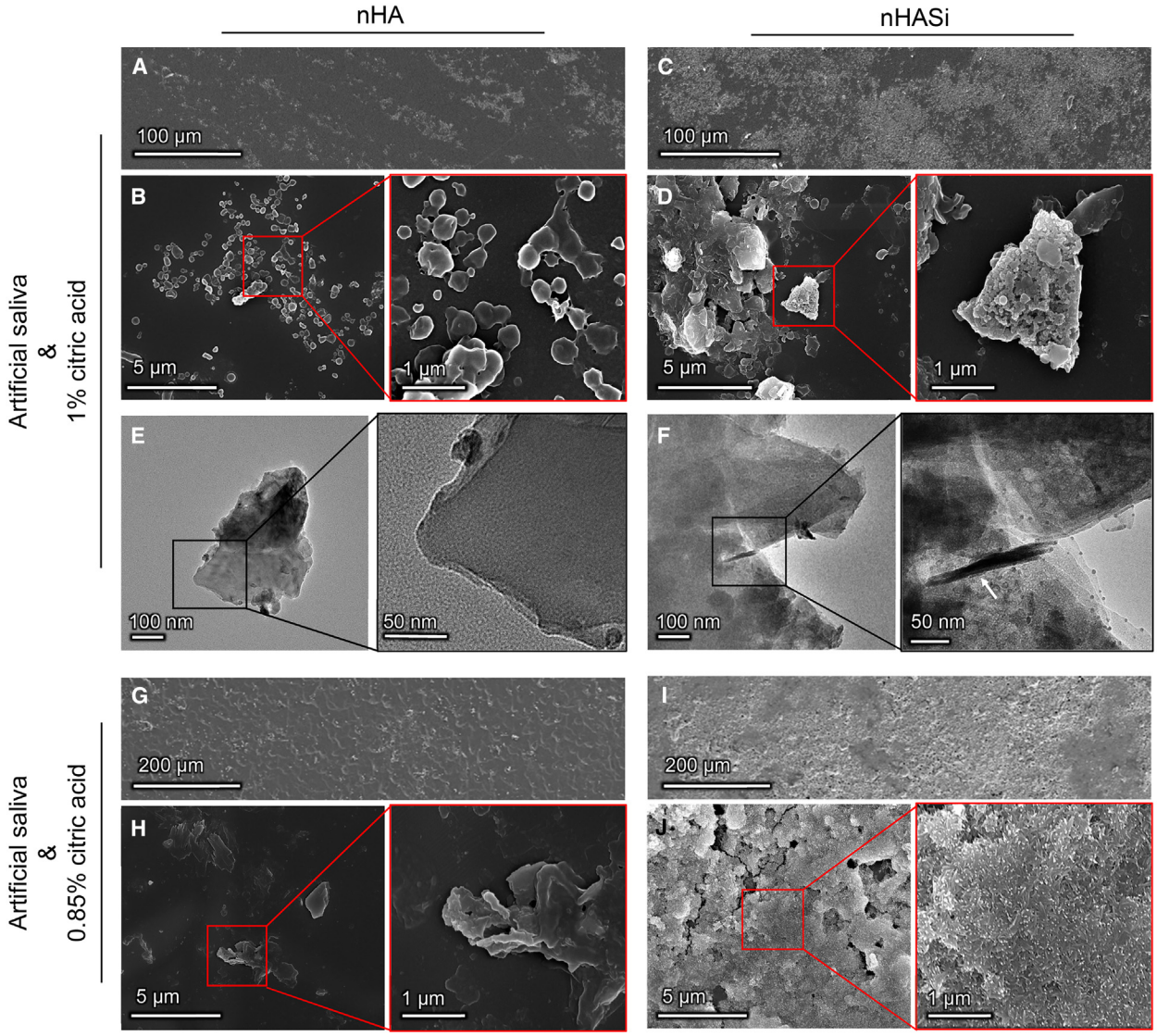


**Figure 4. Biomineralization of nHA and nHASi under cyclic citric acid and artificial salivary treatment for 5 days**

(A–J) SEM images of the de/remineralized particles of (A and B) nHA and (C and D) nHASi treated with artificial saliva and 1 wt % citric acid. TEM results showed that the de/remineralized nHA particle (E) was amorphous, whereas an HA-like crystal (pointed by white arrow) and a great number of dark dots (F), which could be nucleated calcium phosphate were observed in de/remineralized nHASi. When treated with artificial saliva and 0.85 wt % citric acid solution (G–J), although very few de/remineralized nHA particles remained, numerous rod-like HA crystals were generated on the surface of nHASi after 5 days of cyclic de/remineralization. Scale bars are 100 μm for (A) and (C), 5 μm for low magnification and 1 μm for high magnification in (B), (D), (H), and (J), 100 nm for low magnification and 50 nm for high magnification in (E) and (F), and 200 μm for (G) and (I), respectively..

the same as that of the blank group (Figures 6A and 6B), and no significant difference was observed in the live-dead staining assay after 48 h of cultivation (Figure 6C). Hence, to reduce the impact of proliferation differences on the differentiation of DSPCs, we chose culture conditions with a material extract concentration of 3,125 μg/mL for further investigation on odontogenic inductivity. After 21 days of differentiation, the alizarin red staining revealed that both nHA and nHASi contributed to the formation of calcium nodules (Figure 6D), among which, the DSPCs treated with nHASi showed increased size and quantity of calcium nodules. Further immunoblotting analysis of DMP-1 and DSPP (Figures 6E and 6F), two typical markers of odontoblastic differentiation,[38] demonstrated that treatment with nHA and nHASi extracts significantly increased their expression level. More importantly, nHASi exerted a significantly higher promotion on the expression of DMP-1 and DSPP than nHA. Consistent results were noticed by immunofluorescence staining of DMP-1 and DSPP (Figures 6G and 6H). Together, these results suggests that nHASi not only possesses favorable biocompatibility but also exhibits excellent odontogenic inductivity that is able to effectively promote odontoblastic differentiation of DPSCs and calcification of

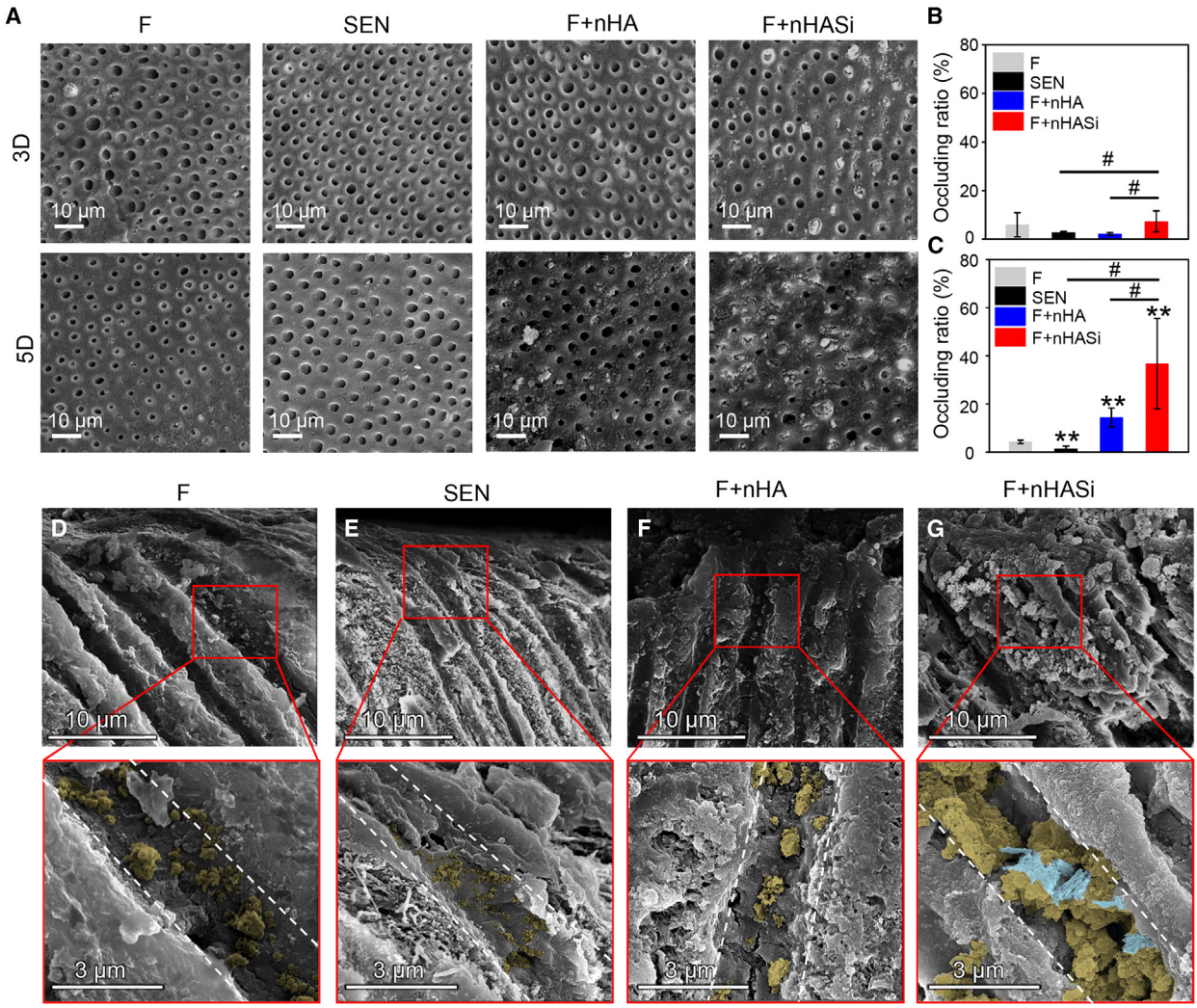


**Figure 5. Dental tubule occlusion by toothpaste containing different minerals**

(A–G) Dental tubule occlusion shown by SEM images of the horizontal surface of the teeth slices after 3 days and 5 days (A) of cyclic de/remineralization treatment and their corresponding occluding ratio statistics. Scale bars are 10 μm. (B and C) showed that the occlusion effect enhanced with treating time in F + nHA and F + nHASi groups, and the F + nHASi group exhibited the most efficient tubule occlusion, in comparison with other groups. Data are means ± SD, $n$ = 10 images collected in each group for statistics, $^{**}p < 0.01$ compared with F group, $\#p < 0.05$ compared with F + nHASi group, by one-way ANOVA with Tukey's multiple comparison test. (D–G) SEM observation on the longitudinal surface of dentin tubules demonstrated that the mineral deposits of nHASi filled up the depth of the tubules, and rod-like HA nanocrystals were exclusively noticed in the F + nHASi group after 5 days. The mineral deposits and HA in tubules were pseudocolored as gold and blue, respectively. And the scale bars are 10 μm for low magnification in the upper panel and 3 μm for high magnification in the lower panel, respectively.

dentin, thereby facilitating the repair of exposed dental tubules. Ceramic materials releasing release silicate ions such as calcium silicate[39,40] and BG[41] have been reported to be able to induce odontoblastic differentiation of DSPCs. Interestingly, in this study, nHASi demonstrated a greater odontogenic inductivity than nHA, possibly attributed to its capability of silicate ion release. Our previous finding demonstrated that nHASi released silicate ions in artificial saliva and remained stable in citric acid solution. Such characteristic may allow nHASi to effectively occlude the dental tubules and simultaneously promote the odontoblastic differentiation of DPSCs through the release of silicate ions in the saliva environment, thereby synergistically inducing reparative dentin to exert long-term effectiveness against DH.

In summary, nHASi was successfully fabricated as a form of nanoparticle with a rod-like HA core and a granular silica coating via precipitation method. The *in vitro* ion release and biomineralization in artificial saliva suggested that the silica coating of nHASi was not only permeable for calcium and phosphate ions release in the neutral condition but also provided active sites for calcium phosphate mineralization to generate HA. Further *in vitro* acid resistance study and cyclic de/remineralization of the particles demonstrated that, due to the silica, nHASi exhibited retarded acid erosion and ion release in comparison

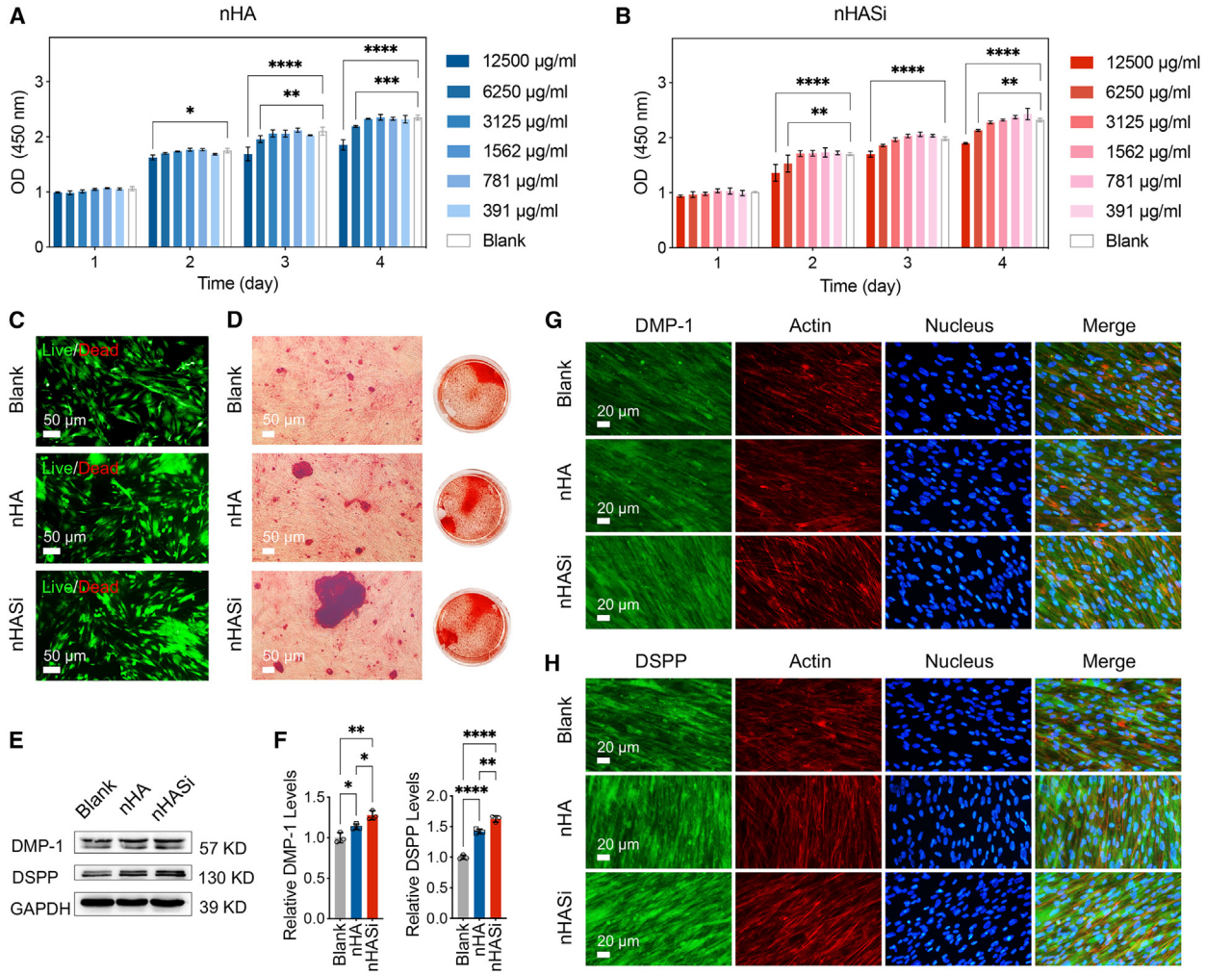


**Figure 6. Cytocompatibility and odontogenic inductivity of nHA and nHASi**

(A and B) The optical density (OD) value detected in CCK-8 assay revealed that both nHA (A) and nHASi (B) extract were of favorable cytocompatibility when their concentration was below 3,125 μg/mL. Data are means ± SD, $n = 3$, $^{*}p < 0.05$, $^{**}p < 0.01$, $^{***}p < 0.001$, $^{****}p < 0.0001$ by two-way ANOVA with Tukey's multiple comparison test. Only groups with significant differences are marked.

(C) Live/dead staining of the DSPCs following 48 h of cultivation with medium containing 3,125 μg/mL of nHA or nHASi extract showed no obvious red-stained dead cells. Scale bars are 50 μm.

(D–H) After 21 days of odontogenic induction, the alizarin red staining of DSPCs (D) (scale bars are 50 μm), the western blot images and (E) corresponding semi-quantitative gray value statistics (F) of DMP-1 and DSPP (data are means ± SD, $n = 3$ blots used for semi-quantitative analysis per group, $^{*}p < 0.05$, $^{**}p < 0.01$, $^{****}p < 0.0001$ by one-way ANOVA with Tukey's multiple comparison test), and the immunofluorescent results of DMP-1 (G) and DSPP (H) showed that both nHA and nHASi promoted odontogenic differentiation of DSPCs, with nHASi exhibiting a more prominent efficiency (scale bars are 20 μm).

with nHA, thereby reserving amorphous calcium phosphate within and surrounding the silica coating to help the subsequent remineralization to form rod-like HA nanocrystals. More importantly, when mixing with toothpaste, nHASi exerted an increasing occluding ratio as the increase of cyclic de/remineralization times and the most effective dentin tubule occlusion among all four groups. Additionally, when the DPSCs were cultured with the materials extract, nHASi not only exhibited outstanding cytocompatibility but also effectively enhanced odontogenic differentiation, offering potential benefits for dentin repair, thus demonstrating promising prospects for long-term DH treatment.

## Limitations of the study

In our work, nHASi has demonstrated prominent acid resistance and long-term dentin tubule occlusion against cyclic de/remineralization *in vitro*. However, we found it difficult to verify the long-term occluding effect of nHASi on dentin tubules in mice or rats. This is due to the necessity of administering anesthesia each time toothpaste containing nHASi is applied for brushing the animals' teeth. Inhalation anesthesia, although relatively mild, hampers effective tooth brushing. On the other hand, injection anesthesia poses high toxicity levels that make it difficult for animals to endure consecutive days of brushing and anesthesia administration. In future work, we

need to find suitable animal models to validate the efficacy of nHASi to endorse its clinical translation.

## RESOURCE AVAILABILITY

### Lead contact

Further information and requests for resources and reagents should be directed to and will be fulfilled by the lead contact, Dr. Shenglong Tan (tansl1989@outlook.com).

### Materials availability

This study did not generate new unique reagents.

### Data and code availability

- All data reported in this paper will be shared by the lead contact upon request.
- This paper does not report original code.
- Any additional information required to reanalyze the data reported in this paper is available from the lead contact upon request.

## ACKNOWLEDGMENTS

This work was supported by the National Natural Science Foundation of China (82271036, 82201133, 82222015, and 82171001), Young Elite Scientist Sponsorship Program by CAST (2022QNRC001), Science Research Cultivation Program of Stomatological Hospital, Southern Medical University (PY2021008), Research Funding from West China School/Hospital of Stomatology Sichuan University (RCDWJS2023-1), and Fundamental Research Funds for the Knowledge Innovation Program of Wuhan (2022020801010085).

## AUTHOR CONTRIBUTIONS

Y.W.: conceptualization, methodology, validation, formal analysis, investigation, data curation, writing – original draft, writing – review and editing, and visualization. S.C.: data curation, writing – review and editing, and validation. M.Z.: data curation and validation. L.C.: conceptualization, methodology, resources, writing – review and editing, and funding acquisition. C.Z.: conceptualization, methodology, writing – review and editing, and funding acquisition. S.T.: conceptualization, methodology, resources, writing – review and editing, funding acquisition, and project administration.

## DECLARATION OF INTERESTS

The authors declare no competing interests.

## STAR★METHODS

Detailed methods are provided in the online version of this paper and include the following:

- KEY RESOURCES TABLE
- EXPERIMENTAL MODEL AND STUDY PARTICIPANT DETAILS
  - Dentin sheets preparation
  - Cell lines and cell culture
- METHOD DETAILS
  - Materials preparation and characterization
  - Adhesion of nHA and nHASi particles on the surface of dentin
  - Ions releasing in artificial saliva and citric acid solution
  - Biomineralization in artificial saliva
  - Acid resistance of nHA and nHASi
  - Biomineralization after cycling de/remineralization
  - Dentin tubules occluding under de/remineralization cycling protocol
  - Evaluation of occluding effectiveness
  - Preparation of nHA and nHASi extract
  - Cytocompatibility evaluation
  - Odontogenic inductivity evaluation
- QUANTIFICATION AND STATISTICAL ANALYSIS

## SUPPLEMENTAL INFORMATION

Supplemental information can be found online at https://doi.org/10.1016/j.isci.2024.111474.

Received: July 4, 2024
Revised: October 22, 2024
Accepted: November 21, 2024
Published: November 23, 2024

## REFERENCES

1. Rong, W.S., Hu, D.Y., Feng, X.P., Tai, B.J., Zhang, J.C., and Ruan, J.P. (2010). A national survey on dentin hypersensitivity in Chinese urban adults. Appl. Psychol. Meas. *45*, 141–145. https://doi.org/10.3724/SP.J.1077.2010.01195.
2. Paschos, E. (2014). Prevalence of dentine hypersensitivity and study of associated factors: a European population-based cross-sectional study. J. Orofac. Orthop. *75*, 78–84. https://doi.org/10.1007/s00056-013-0196-2.
3. Mantzourani, M., and Sharma, D. (2013). Dentine sensitivity: Past, present and future. J. Dent. *41*, S3–S17. https://doi.org/10.1016/S0300-5712(13)70002-2.
4. Orchardson, R., and Gillam, D.G. (2006). Managing dentin hypersensitivity. J. Am. Dent. Assoc. *137*, 990–1029. https://doi.org/10.14219/jada.archive.2006.0321.
5. Degli Esposti, L., Ionescu, A.C., Brambilla, E., Tampieri, A., and Iafisco, M. (2020). Characterization of a Toothpaste Containing Bioactive Hydroxyapatites and In Vitro Evaluation of Its Efficacy to Remineralize Enamel and to Occlude Dentinal Tubules. Materials *13*, 2928. https://doi.org/10.3390/ma13132928.
6. Zhong, Y., Liu, J., Li, X., Yin, W., He, T., Hu, D., Liao, Y., Yao, X., and Wang, Y. (2015). Effect of a novel bioactive glass-ceramic on dentinal tubule occlusion: an in vitro study. Aust. Dent. J. *60*, 96–103. https://doi.org/10.1111/adj.12241.
7. Lee, M., Lee, Y.S., Shon, W.J., and Park, J.C. (2023). Physiologic dentin regeneration: its past, present, and future perspectives. Front. Physiol. *14*, 1313927. https://doi.org/10.3389/fphys.2023.1313927.
8. Yu, T., Wang, Y., Cai, Q., and Wu, L. (2020). Efficacy of Ca2+-or PO43–conjugated mesoporous silica nanoparticles on dentinal tubule occlusion: an in-vitro assessment. Ann. Transl. Med. *8*, 173–180. https://doi.org/10.21037/atm.2020.01.98.
9. Medvecky, L., Giretova, M., and Sopcak, T. (2013). Preparation and properties of tetracalcium phosphate–monetite biocement. Mater. Lett. *100*, 137–140. https://doi.org/10.1016/j.matlet.2013.03.025.
10. Aoba, T. (2004). Solubility properties of human tooth mineral and pathogenesis of dental caries. Oral Dis. *10*, 249–257. https://doi.org/10.1111/j.1601-0825.2004.01030.x.
11. Matos, A.B., Palma, R.G., Saraceni, C.H., and Matson, E. (1997). Effects of acid etching on dentin surface: SEM morphological study. Braz. Dent. J. *8*, 35–41.
12. Featherstone, J.D.B., and Lussi, A. (2006). Understanding the chemistry of dental erosion. Monogr. Oral Sci. *20*, 66. https://doi.org/10.1159/000093351.
13. Reyes-Gasga, J., Martínez-Piñeiro, E.L., Rodríguez-Álvarez, G., Tiznado-Orozco, G.E., García-García, R., and Brès, E.F. (2013). XRD and FTIR crystallinity indices in sound human tooth enamel and synthetic hydroxyapatite. Mater. Sci. Eng., C *33*, 4568–4574. https://doi.org/10.1016/j.msec.2013.07.014.
14. Lopes, M.B., Sinhoreti, M.A.C., Gonini Júnior, A., Consani, S., and Mccabe, J.F. (2009). Comparative study of tubular diameter and quantity for human and bovine dentin at different depths. Braz. Dent. J. *20*, 279–283. https://doi.org/10.1590/S0103-64402009000400003.

15. Rahaman, M.N., Day, D.E., Bal, B.S., Fu, Q., Jung, S.B., Bonewald, L.F., and Tomsia, A.P. (2011). Bioactive glass in tissue engineering. Acta Biomater. *7*, 2355–2373. https://doi.org/10.1016/j.actbio.2011.03.016.

16. Rajesh, K.S., Hedge, S., Arun Kumar, M.S., and Shetty, D.G. (2012). Evaluation of the efficacy of a 5% calcium sodium phosphosilicate (Novamin) containing dentifrice for the relief of dentinal hypersensitivity: a clinical study. Indian J. Dent. Res. *23*, 363–367. https://doi.org/10.4103/0970-9290.102228.

17. Fernando, D., Attik, N., Pradelle-Plasse, N., Jackson, P., Grosgogeat, B., and Colon, P. (2017). Bioactive glass for dentin remineralization: A systematic review. Mater. Sci. Eng., C *76*, 1369–1377. https://doi.org/10.1016/j.msec.2017.03.083.

18. Tang, F., Li, L., and Chen, D. (2012). Mesoporous silica nanoparticles: synthesis, biocompatibility and drug delivery. Adv. Mater. *24*, 1504–1534. https://doi.org/10.1002/adma.201104763.

19. Steven, C.R., Busby, G.A., Mather, C., Tariq, B., Briuglia, M.L., Lamprou, D.A., Urquhart, A.J., Grant, M.H., and Patwardhan, S.V. (2014). Bio-inspired silica as drug delivery systems and their biocompatibility. J. Mater. Chem. B *2*, 5028–5042. https://doi.org/10.1039/c4tb00510d.

20. Hosseinpour, S., Walsh, L.J., and Xu, C. (2020). Biomedical application of mesoporous silica nanoparticles as delivery systems: a biological safety perspective. J. Mater. Chem. B *8*, 9863–9876. https://doi.org/10.1039/D0TB01868F.

21. Hoang Thi, T.T., Cao, V.D., Nguyen, T.N.Q., Hoang, D.T., Ngo, V.C., and Nguyen, D.H. (2019). Functionalized mesoporous silica nanoparticles and biomedical applications. Mater. Sci. Eng., C *99*, 631–656. https://doi.org/10.1016/j.msec.2019.01.129.

22. Tian, L., Peng, C., Shi, Y., Guo, X., Zhong, B., Qi, J., Wang, G., Cai, Q., and Cui, F. (2014). Effect of mesoporous silica nanoparticles on dentinal tubule occlusion: an in vitro study using SEM and image analysis. Dent. Mater. J. *33*, 125–132. https://doi.org/10.4012/dmj.2013-215.

23. Li, X., Li, X., Wang, S., Leung, K.C.-F., Zhang, C., and Jin, L. (2018). Infiltration and Profiles of Mesoporous Silica Nanoparticles in Dentinal Tubules. ACS Biomater. Sci. Eng. *4*, 1428–1436. https://doi.org/10.1021/acsbiomaterials.7b00919.

24. Chiang, Y.C., Lin, H.P., Chang, H.H., Cheng, Y.W., Tang, H.Y., Yen, W.C., Lin, P.Y., Chang, K.W., and Lin, C.P. (2014). A mesoporous silica biomaterial for dental biomimetic crystallization. ACS Nano *8*, 12502–12513. https://doi.org/10.1021/nn5053487.

25. Karumuri, S., Mandava, J., Pamidimukkala, S., Uppalapati, L.V., Konagala, R.K., and Dasari, L. (2020). Efficacy of hydroxyapatite and silica nanoparticles on erosive lesions remineralization. J. Conserv. Dent. *23*, 265–269. https://doi.org/10.4103/JCD.JCD_182_20.

26. Yu, J., Yang, H., Li, K., Lei, J., Zhou, L., and Huang, C. (2016). A novel application of nanohydroxyapatite/mesoporous silica biocomposite on treating dentin hypersensitivity: An in vitro study. J. Dent. *50*, 21–29. https://doi.org/10.1016/j.jdent.2016.04.005.

27. Madupalli, H., Pavan, B., and Tecklenburg, M.M.J. (2017). Carbonate substitution in the mineral component of bone: Discriminating the structural changes, simultaneously imposed by carbonate in A and B sites of apatite. J. Solid State Chem. *255*, 27–35. https://doi.org/10.1016/j.jssc.2017.07.025.

28. Stoch, A., Jastrz, W., Brożek, A., Trybalska, B., Cichocińska, M., and Szarawara, E. (1999). FTIR monitoring of the growth of the carbonate containing apatite layers from simulated and natural body fluids. J Mol Struct *s*. J. Mol. Struct. *511*, 287–294. https://doi.org/10.1016/S0022-2860(99)00170-2.

29. Al-Kady, A.S., Gaber, M., Hussein, M.M., and Ebeid, E.Z.M. (2011). Nanostructure-loaded mesoporous silica for controlled release of coumarin derivatives: a novel testing of the hyperthermia effect. Eur. J. Pharm. Biopharm. *77*, 66–74. https://doi.org/10.1016/j.ejpb.2010.10.007.

30. Wang, L., Shen, A., and Yao, J. (2020). Effect of different coarse aggregate surface morphologies on cement emulsified asphalt adhesion. Construct. Build. Mater. *262*, 120030. https://doi.org/10.1016/j.conbuildmat.2020.120030.

31. Kaidonis, J.A. (2012). Oral diagnosis and treatment planning: part 4. Non-carious tooth surface loss and assessment of risk. Br. Dent. J. *213*, 155–161. https://doi.org/10.1038/sj.bdj.2012.722.

32. Sousa, S.M.G.d., and Silva, T.L. (2005). Demineralization effect of EDTA, EGTA, CDTA and citric acid on root dentin: a comparative study. Braz. Oral Res. *19*, 188–192. https://doi.org/10.1590/s1806-83242005000300006.

33. Degli Esposti, L., Zheng, K., Piancastelli, A., Ionescu, A.C., Adamiano, A., Boccaccini, A.R., and Iafisco, M. (2024). Composite materials of amorphous calcium phosphate and bioactive glass nanoparticles for preventive dentistry. Ceram. Int. *50*, 593–602. https://doi.org/10.1016/j.ceramint.2023.10.137.

34. Abou Neel, E.A., Aljabo, A., Strange, A., Ibrahim, S., Coathup, M., Young, A.M., Bozec, L., and Mudera, V. (2016). Demineralization-remineralization dynamics in teeth and bone. Int. J. Nanomed. *11*, 4743–4763. https://doi.org/10.2147/ijn.S107624.

35. Fabay, R.V., Tumbokon, B.L., and Serrano, A.E. (2020). Effects of dietary pH and acid source on growth and feed efficiency of the Nile Tilapia, Oreochromis niloticus fry. Oreochromis niloticus fry. Isr J Aquacult-bamid *72*, 1114685. https://doi.org/10.46989/001C.19031.

36. Chen, L.W., Gu, S., and Jia, X.Y. (2015). Occluding effects of desensitizer containing NovaMin combined with fluor protector on dentinal tubules:an in vitro study. Shanghai kou Qiang yi xue= Shanghai Journal of Stomatology *24*, 535–540.

37. Tan, S., Chen, S., Wang, Y., Wu, F., Shi, Y., Wang, J., Du, Y., and Zhang, S. (2020). Enhanced effect of nano-monetite hydrosol on dentin remineralization and tubule occlusion. Dent. Mater. *36*, 816–825. https://doi.org/10.1016/j.dental.2020.03.028.

38. Zhan, P., Zhang, X., Xie, Z., Chen, L., Huang, S., Huang, Q., Lin, Z., and Wang, R. (2024). Nicotinamide Riboside Modulates HIF-1 Signaling to Maintain and Enhance Odontoblastic Differentiation in Human Dental Pulp Stem Cells. Stem Cell. *42*, 116–127. https://doi.org/10.1093/stmcls/sxad083.

39. Liu, C.H., Hung, C.J., Huang, T.H., Lin, C.C., Kao, C.T., and Shie, M.Y. (2014). Odontogenic differentiation of human dental pulp cells by calcium silicate materials stimulating via FGFR/ERK signaling pathway. Mater. Sci. Eng., C *43*, 359–366. https://doi.org/10.1016/j.msec.2014.06.025.

40. Ghosh, A., and Chowdhury, S. (2013). Sterilization and Disinfection of Extracted Human Teeth for Institutional Use. Int J Clin Dent Sci *4*, 9–12. https://doi.org/10.1002/ar.1090070102.

41. Zhu, L., Li, J., and Dong, Y. (2021). Effect of mesoporous bioactive glass on odontogenic differentiation of human dental pulp stem cells. PeerJ *9*, e12421. https://doi.org/10.7717/peerj.12421.

42. Medvecky, L., Stulajterova, R., Giretova, M., Mincik, J., Vojtko, M., Balko, J., and Briancin, J. (2018). Effect of tetracalcium phosphate/monetite toothpaste on dentin remineralization and tubule occlusion in vitro. Dent. Mater. *34*, 442–451. https://doi.org/10.1016/j.dental.2017.11.022.

## STAR★METHODS

### KEY RESOURCES TABLE

| REAGENT or RESOURCE | SOURCE | IDENTIFIER |
|---|---|---|
| **Antibodies** | | |
| Mouse monoclonal anti-DSPP | Santa Cruz | Cat# sc-73632; RRID: AB_2230660 |
| Mouse monoclonal anti-DMP-1 | Santa Cruz | Cat# sc-73633; RRID: AB_2292808 |
| HRP-conjugated Goat Anti-Mouse IgG(H + L) | Proteintech | Cat# SA00001-1; RRID: AB_2722565 |
| Alexa Fluor 488 conjugated Goat Anti-Mouse IgG(H + L) | Servicebio | Cat# GB25301; RRID: AB_2904018 |
| **Biological samples** | | |
| Human dentin sheets | Stomatology Hospital, Southern Medical University | N/A |
| **Chemicals, peptides, and recombinant proteins** | | |
| Acetic acid | Sinopharm Chemical Co. Ltd of China | Cat# 10000208 |
| Calcium hydroxide | Sinopharm Chemical Co. Ltd of China | Cat# 20011618 |
| Phosphoric acid | Sinopharm Chemical Co. Ltd of China | Cat# 10015408 |
| Tetraethylorthosilicate (TEOS) | Sinopharm Chemical Co. Ltd of China | Cat# 80124118 |
| Sodium chloride | Sinopharm Chemical Co. Ltd of China | Cat# 10019308 |
| Potassium chloride | Sinopharm Chemical Co. Ltd of China | Cat# 10016308 |
| Calcium chloride dihydrate | Sinopharm Chemical Co. Ltd of China | Cat# 20011160 |
| Sodium dihydrogen phosphate dihydrate | Sinopharm Chemical Co. Ltd of China | Cat# 20040718 |
| Sodium sulfide | Sinopharm Chemical Co. Ltd of China | Cat# 10020660 |
| Citric acid | Sinopharm Chemical Co. Ltd of China | Cat# 10001608 |
| Anhydrous ethanol | Sinopharm Chemical Co. Ltd of China | Cat# 10009218 |
| αMEM | Gibco | Cat# 12571063 |
| Penicillin-streptomycin | Gibco | Cat# 15140122 |
| Fetal bovine serum | Cyagen Bioscience Inc. | Cat# FBSSR-01021 |
| Ascorbic acid | Sigma-Aldrich | Cat# A4544-25G |
| β-glycerophosphate | Sigma-Aldrich | Cat# G9422-10G |
| Dexamethasone | Sigma-Aldrich | Cat# D4902-100MG |
| Triton X-100 | Sigma-Aldrich | Cat# T8787-50ML |
| Bovine serum albumin | Sigma-Aldrich | Cat# V900933-100G |
| Alizarin red solution | Cyagen Bioscience Inc. | Cat# ALIR-10001 |
| Rhodamine B labeled phalloidin | Invitrogen™ | Cat# R415 |
| DAPI | Servicebio | Cat# G1012-10ML |
| Paraformaldehyde solution | Servicebio | Cat# G1101-500ML |
| **Critical commercial assays** | | |
| Phosphate fluorometric assay kit | BioVision, Inc. | Cat# K420-100 |
| Silicate assay kit | HKT™, Inc. China | https://www.hkchemistry.com/show/21326.html |
| CCK-8 assay kit | Beyotime | Cat# C0038 |
| Live dead assay kit | Beyotime | Cat# C2015S |
| **Experimental models: Cell lines** | | |
| Human dental pulp stem cells | iCell Bioscience Inc. | HUM-iCell-m003 |
| **Software and algorithms** | | |
| JADE 6.5 | International Center for Diffraction Data, ICDD | N/A |
| Origin 8.0 | Originlab Company | N/A |

(*Continued on next page*)

*Continued*

| REAGENT or RESOURCE | SOURCE | IDENTIFIER |
|---|---|---|
| Prism 9 | Graphpad | N/A |
| ImageJ | NIH | N/A |
| Other | | |
| X-ray diffraction | PANalytical B.V., Holland | X'Pert PRO |
| X-ray Fluorescence | EDAX, Inc | Orbis PC |
| Fourier transform infrared | Bruker, Germany | Vertex 70 |
| Scanning electron microscopy | FEI, Holland | Nova NanoSEM 450 |
| Transmission electron microscope | FEI, Holland | Tecnai G2 F30 |
| Fluorescence microscope | Nexcpoe, China | NE910 |

## EXPERIMENTAL MODEL AND STUDY PARTICIPANT DETAILS

### Dentin sheets preparation

Due to orthodontic reasons, the extracted teeth donated from Stomatology Hospital, Southern Medical University, were used in this study. All experiments were performed in compliance with the policy of the Ethics Committee of Stomatology Hospital, Southern Medical University. All 20 donated teeth (from 10 males and 10 females, 18–25 years old) were sterilized by using 3% sodium hypochlorite solution for 20 min before use.[40] Dentin sheets with about 1mm in thickness was obtained by cutting the tooth using a diamond disk attached to micro-motor. Each tooth can produce 2–3 dentin sheets and a total of 49 dentin sheets were obtained. Then the surface of dentin sheets was grounded using 800, 1500, 2000 and 3000-grit silicon carbide paper in sequence, and the dentin tubules were opened by soaking the sheets in 35 wt. % phosphoric acid for 2 min. All dentin sheets were kept in sterile saline till tested.

### Cell lines and cell culture

Human dental pulp stem cells (DPSCs) (HUM-iCell-m003) were purchased from iCell Bioscience Inc, Shanghai, China, and incubated with a culture medium (CM) consist of αMEM (Gibco), 10% fetal bovine serum (FBS) (Cyagen Biosciences Inc.) and 1% penicillin-streptomycin (Gibco), in a humidified incubator at 37°C with 5% $CO_2$. The CM was replaced every 3 days. Cells from passages 3–6 were utilized for cytocompatibility and odontogenic inductivity evaluation of the nHA and nHASi extracts.

## METHOD DETAILS

### Materials preparation and characterization

Nano hydroxyapatite (nHA) was fabricated as our previous study[37] with some modification. In detail, with mechanical stirring at 60°C, 99.8 g acetic acid was added to the 246.6 mL calcium hydroxide suspension (the molar ratio of COOH and OH was 1:1). Then 139mL of 14 wt % phosphoric acid solution was added dropwise, to achieve the final concentration of 3.45 mol/L, 3.45 mol/L and 0.41 mol/L for acetic acid, calcium hydroxide and phosphoric acid, respectively. After reaction for 4h, the obtained mixture was filtered and washed with deionized water for 3 times. The synthesis process of nHASi was similar to that in nHA, except that 103.6 mL of 0.93 mol/L tetraethylorthosilicate (TEOS) was added dropwise within about 30 min after the addition of phosphoric acid.

For the following characterizations and experiments, the synthesized nHA and nHASi were prepared in two forms, hydrosol and powder, respectively. For the hydrosol, the filter cake of nHA or nHASi was homogeneously dispersed in 200 mL deionized water by ultrasonic treatment to get an as-prepared hydrosol. In order to determine the concentration, 1 mL of the as-prepared hydrosol was collected and centrifuged at 12000 rpm for 5 min. After removing the supernatant, the precipitation was dried at 60°C until getting a constant weight of X g. The concentration of the as-prepared hydrosol is determined to be X g/mL. A hydrosol of a specific concentration can be obtained by diluting the as-prepared hydrosol with X g/mL using deionized water. To obtain the nHA and nHASi powders, the filter cakes were dried at 60°C and grinded with mortar. All chemical reagents used in this section was purchased from Sinopharm Chemical Co., Ltd of China. The chemical compositions, quantity of elements, bond configuration, surface morphology and microstructure of nHA and nHASi were characterized using X-ray diffraction (XRD, X'Pert PRO, PANalytical B.V., Holland), X-ray Fluorescence (XRF, EDAX, Inc), Fourier transform infrared (FTIR, Vertex 70, Bruker, Germany), Scanning electron microscopy (SEM, FEI, Holland) and Transmission electron microscope (TEM, Tecnai G2 F30, FEI, Holland) respectively.

### Adhesion of nHA and nHASi particles on the surface of dentin

nHA and nHASi hydrosols, each with a concentration of 0.5 mg/mL, were prepared for this test. A total of nine dentin sheets with open tubules were utilized in this experiment. For the adhesion experiment, six dentin sheets were assigned to the nHA and nHASi hydrosol groups, with three dentin sheets per group. These sheets were brushed for 3 min using electric toothbrush (Shuguang of Yangzhou city Toothbrush factory, China) with the respective hydrosol materials. Following the brushing, the sheets were rinsed twice with deionized water and dried at 60°C before observation using SEM. Additionally, three untreated dentin sheets served as the Blank group and were also observed using SEM.

### Ions releasing in artificial saliva and citric acid solution

Ions releasing was conducted by soaking 0.01g nHA or nHASi powders (passing through 150 mesh sieves) into centrifuge tube containing 5 mL of artificial saliva, which consist of 400 mg/L NaCl, 400 mg/L KCl, 79.5 mg/L $CaCl_2 \cdot 2H_2O$, 780 mg/L $NaH_2PO_4 \cdot 2H_2O$, and 5 mg/L $Na_2S$ according to ISO10271, or 1 wt. % citric acid solution[32] at 37°C. The pH value of artificial saliva and citric acid solution were detected to be 6.8 and 2.23 using acidometer (FE28, Mettler Toledo, Germany). At different time points, centrifugation (4000 rpm, 5 min) was performed before gently collecting 1 mL of the supernatant for detection. 1 mL of artificial saliva or 1 wt. % citric acid solution was added to the centrifuge tube to fill the volume to 5 mL. The materials were dispersed by vortex and set for ions release until next time point. Three parallel samples per group was designed. The concentration of $Ca^{2+}$, $PO_4^{3-}$ and $SiO_3^{2-}$ were determined by Atomic emission spectrometry (ICP-AES, PerkinElmer Optima 2000), Phosphate fluorometric assay kit (BioVision, Inc., USA) and Silicate determining kit (HKT, Inc., China), respectively. Prior to quantifying the calcium ions, a standard curve for calcium ions was established. Specifically, a series of calcium ion standard solutions were prepared at concentrations of 0 μg/mL, 2 μg/mL, 4 μg/mL, 6 μg/mL, 8 μg/mL and 10 μg/mL, and the absorbance values of these solution were measured using ICP-AES. The standard curve for calcium ions was then constructed based on the various calcium ion concentration and their corresponding absorbance values. Subsequently, the absorbance value of the collected supernatant was determined by ICP-AES, and the calcium concentration of the collected supernatant at each predetermined time point "$c_n$" was obtained according to the standard curve. Then the accumulated calcium concentration "$C_n$" at each predetermined time point can be calculated as follow:

$$C_n = \frac{\left(\sum_{i=1}^{n-1} ci + 5c_n\right)}{5}$$

The concentration of $PO_4^{3-}$ or $SiO_3^{2-}$ in the collected supernatant was determined following the product manual. And the calculation of their accumulated concentration was consistent with that of calcium ions.

### Biomineralization in artificial saliva

0.01g nHA or nHASi powders were soaked in 4 mL artificial saliva at 37°C. Then the solutions were refreshed every two days. After 7 and 14 days, the powers were collected by centrifugation at 4000 rpm for 5 min. Then 1 mL anhydrous ethanol (analytical reagent) was added to terminate the mineralization. Subsequently, after centrifugation again, powers were dried in an oven at 60°C for 12 h. The surface morphology and phase composite were then analyzed by SEM and XRD.

### Acid resistance of nHA and nHASi

10 μL nHA or nHASi hydrosol with a concentration of 0.5 mg/mL was added to the cleaned silicon wafer. Once dried at room temperature, 10 μL 1 wt. % citric acid solution was added and kept for 30 s at room temperature. Citric acid on silicon wafer was then removed by gently washing three times with deionized water. Subsequently, silicon wafer was dried in an oven at 60°C for 12 h before using SEM to observe the surface morphology of materials remaining on the silicon wafer. The residual minerals on the silicon wafer were collected by sonicating in anhydrous ethanol for 1min, and the micro-structure was further characterized using TEM.

### Biomineralization after cycling de/remineralization

The biomineralization process was conducted on cleaned silicon wafers. The de/remineralization cycling protocol consisted of two cycles per day, with each cycle comprising three steps: 1: Adding 10μL of nHA or nHASi hydrosol at a concentration of 0.5 mg/mL on the cleaned silicon wafers, followed by drying at room temperature. 2. Soaking the silicon wafers in the artificial saliva for 12 h. 3: rinsing the silicon wafers with distilled water and subsequently treating them with citric acid solution at concentration of 0.25 wt. %, 0.4 wt. %, 0.55 wt. %, 0.7 wt. %, 0.85 wt. % or 1 wt. % for 1 min, respectively. The silicon wafers were then washed again with deionized water. This cycling process is repeated continuously, staring from step 1. After repeating 10 cycles (5 days), the silicon wafers were collected and rinsed with distilled water. The the remaining minerals on the silicon wafers were characterized using SEM and TEM.

### Dentin tubules occluding under de/remineralization cycling protocol

Four toothpastes were designed for dentin tubules occluding. Darlie toothpaste (Holly Chemical (Zhongshan) Co., Ltd., CHN) and Sensodyne anti-sensitivity toothpaste (Novamin 5%) were used as control groups, named as F group and SEN group, respectively. For the experimental groups, Darlie toothpastes mixed 2 wt. % nHA or nHASi hydrosol were prepared using stirring deaerator (Sienox, SIE-CSOOSL) and named as F + nHA and F + nHASi group, respectively. A total 40 dentin sheets with open tubules were choose, with 5 dentin sheets allocated to each group, and conduced the de/remineralization cycling for 3 or 5 days. The de/remineralization cycling was modified according to a reported study[42] as follows: first, dentin sheets were brushed with pea-sized experimental toothpastes for 3min using electric toothbrushes, and then soaked into 2 mL artificial saliva at 37°C for 6h. After that, dentin sheets were collected and treated with 1% citric acid solution for 5 min, and then soaked into artificial saliva for 1h. Subsequently, dentin sheets were brushed with pea-sized experimental toothpastes for 3 min and mineralized in artificial saliva for 11 h, and then treated with 1% citric acid solution for 5 min, and then soaked into artificial saliva for 1 h. the de/remineralization cycling in detail was showed in Figure S1.

### Evaluation of occluding effectiveness

After 3 and 5 days, dentin sheets were collected, dried in oven at 60°C for 24 h and observed by SEM. 5 dentin sheets per group and 2–3 images per dentin sheet with the magnification of 2400× were obtained. Ten images were collected in each group for statistics ultimately. Then the occluding rate was calculated as the following formula:

$$\text{Occluding ratio}\ (\%) = (\text{the number of closed tubules} / \text{total number of tubules}) \times 100$$

The definition of a "closed tubule" was that the enclosed area of the dentinal tubule is more than 90%, which was assessed using ImageJ.

Additionally, the longitudinal surface of the dentin tubules were examined by SEM. For this, dentin sheets were cut in a direction perpendicular to obtain longitudinal section. Subsequently, the longitudinal section was placed facing upwards, and observed by SEM after gold spraying.

### Preparation of nHA and nHASi extract

1 g of nHA or nHASi powder passing through 150 mesh sieves was autoclaved and immersed in 20 mL of FBS-free CM. After incubation at 37°C for 72 h, the extract was collected through a 0.22 μm filter (Millipore) and diluted with medium for further use.

### Cytocompatibility evaluation

The DSPCs were seeded in 96-well plates (Corning) at a density of $5\times 10^3$ cells/well (3 wells per group) and allowed to attach for 1 day before replacing the medium with CM containing 12500 μg/mL, 6250 μg/mL, 3125 μg/mL, 1562 μg/mL, 781 μg/mL, 391 μg/mL of nHA or nHASi extract. The DSPCs were subsequently cultured for an additional 1, 2, 3, and 4 days, with the CCK-8 assay being performed each day to assess the impact of nHA and nHASi on cell viability and proliferation. Live dead assay was also performed by culturing DSPCs in glass bottom cell culture dishes (NEST Biotechnology Co.) with CM containing 3125 μg/mL of nHA or nHASi extract for 24 h, followed by staining with calcein-AM and propidium iodide (PI) and subsequent observation using a fluorescence microscope (NE910, Nexcpoe, China). The CCK-8 assay kit and Live dead assay kit were both purchased from Beyotime.

### Odontogenic inductivity evaluation

DSPCs were preincubated in 6-well plates (Corning) at a density of $2.5 \times 10^4$ cells/well. When the cell confluent rate reached about 70%, the CM was replaced with a reported odontoblastic differentiation induction medium (OM)[38] consist of CM with 50 μg/mL of ascorbic acid (Sigma- Aldrich), 10 mM of β-glycerophosphate (Sigma-Aldrich), and 10 nM of dexamethasone (Sigma-Aldrich), as well as OM containing 3125 μg/mL of nHA or nHASi extract. The medium was replaced every three days throughout the 21-day period of differentiation induction. Subsequently, the cells were fixed using a 4% paraformaldehyde solution and stained with alizarin red to visualize calcium nodule formation under an optical microscope. Meanwhile, cell lysis was performed on ice to extract total protein for subsequent Western blot (WB) analysis of DMP-1 and DSPP, two characteristic proteins of odontoblastic differentiation. The gray values of blots were determined using ImageJ for semi-quantitative analysis. For immunofluorescence (IF) observation, DSPCs were differentiated in glass bottom cell culture dishes for 21 days, followed by fixing with 4% paraformaldehyde at 4°C, permeablizing by 0.3% Triton X-100, and blocking with 1% BSA at room temperature. The cells were incubated with the primary antibody of DMP-1 and DSPP and then with Alexa Fluor 488 labeled secondary antibody. Subsequently, the cytoskeleton and nucleus were stained with Rhodamine B labeled phalloidin and DAPI, respectively. The expression of DMP-1 and DSPP was observed using fluorescence microscope. The primary antibody of DMP-1 (sc-73633) and DSPP (sc-73632) were from Santa Cruz and utilized in WB and IF assays followed the instruction.

## QUANTIFICATION AND STATISTICAL ANALYSIS

All quantitative data were expressed as mean ± standard deviation (SD) in this article. The releasing of $Ca^{2+}$, $PO_4^{3-}$, and $SiO_3^{2-}$ ions in artificial saliva and citric acid solution were plotted using Origin 8.0 and the statistical details are shown in the legends of

Figures 2 and 3. The graphic production and the statistical analysis of dentin tubules occluding ratio, cell viability and proliferation of DSPCs, as well as the gray values of western blots were accomplished using Prism 9 (GraphPad). For occluding ratio and gray values of western blots, a one-way analysis of variance with Tukey's multiple comparison test was used. For cell viability and proliferation, a two-way analysis of variance with Tukey's multiple comparison test was used. The details including the number of parallel samples and the *p* values can be found in the legends of Figures 5 and 6.